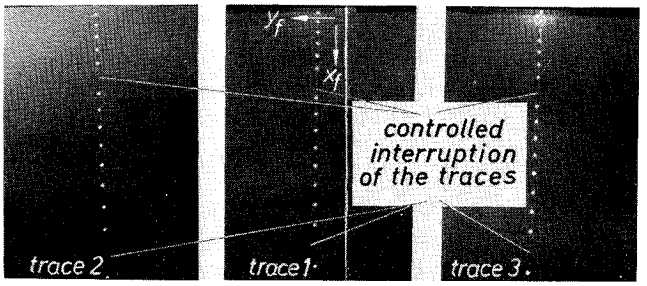

Fig. 2. Parts of the unrolled film with the three traces of points.

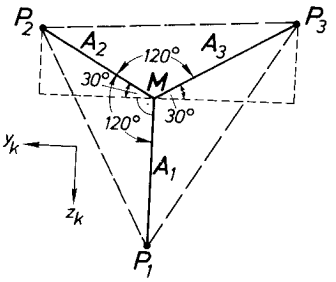

Fig. 3 Plan surface spanned in space by three belonging points.

Aerodynamic Forces and Moments

Positions and attitudes and the fixed time interval are known. The velocity of the model is obtained from the coordinates of two locations, and from three locations the three components of the acceleration may be calculated. Knowing the mass of the model, aerodynamic forces may then be calculated. The moments are calculated in standard fashion using the moments of inertia of the model.

Another approach to obtain the acceleration of the model is to compute the function of time-dependent model-location, for example by a Guass-Approximation, and then take the second derivative. This method may lead to a better accuracy to avoid statistical computing and reading errors.

The acceleration expressed by the different model locations is

$$a = \frac{(s_3 - s_2) - (s_2 - s_1)}{\Delta t^2} \tag{4}$$

Newton's equation for the differences in model location

$$s_3 - 2s_2 + s_1 = \frac{F}{m} \Delta t^2 \tag{5}$$

These differences have to be large compared with the reading error of the coordinates of the light points on the film. For example, for an accuracy of ± 0.05 mm and a largest permissible error of ±1% the differences have to be $s_3 - 2s_2 + s_1 = 20$ mm. Thus from the previous formula we have the postulation: aerodynamic forces F: to be large; model mass-- m: to be low; time interval Δt: to be large. The last demand contradicts the requirement for redundancy.

Aerodynamic forces for a specific model and specific flow conditions are fixed to the same order of magnitude. The only way to get sufficiently large differences is to lower the model mass which sometimes is not possible. To overcome this problem, the Gauss-Approximation may be applied. In this case the time interval Δt is comparable to the half of the registrated testing time; that means, s_1 is the coordinate of the first registrated point, s_3 is the coordinate of the last point or the preceding one, depending on whether there is a straight number of registrated points or not, s_2 is the point between s_1 and s_3.

To get optimal test results the time required for the model in passing through the registrating section should be equal to the time of fully established flow in this section. The length of this registrating test section is fixed by the dimension of the films and there exists a clear relationship between this length, the testing time and the acceleration:

$$s = \int\int a\, dt^2 = \int\int \frac{F}{m}\, dt^2 = \frac{F}{m} t^2 \tag{6}$$

(assuming that during one test the aerodynamic forces are almost constant).

For this case the highest accuracy ever possible (related to reading errors) can be calculated. For optimum conditions, the time interval Δt is not only half the registrated testing time but half the running time of the tunnel. With this the differences in model location are

$$s_3 - 2s_2 + s_1 = \frac{F}{m} \frac{t^2}{4} = \frac{s}{4} \tag{7}$$

For a registration length of the film of 120 mm and a reading error of 0.05 mm the possible evaluation error amounts to 2/3%.

On the other hand, because the length of the flight path and the testing time are fixed, there is also a fixed value for F/m. That means the weight of the model depends on the aerodynamic forces, mainly on the drag. For values of $F/m < s/t^2$ the registration time of the model flight is partially out of the testing time. So we have the postulation

$$F/m \geq s/t^2 \tag{8}$$

where the limiting value is identical with the optimum conditions.

References

[1] Requardt, G. and Kabelitx, H. P., "Development of and Preliminary Investigations on a Free Flight Testing System for a Gun Tunnel," *ICIASF'71 Record,* 1971, pp. 14-19.

[2] Requardt, G. and Wyborny, W., "Aerodynamic Free Flight Testing for a Gun Tunnel," *ICIASF'73 Record,* 1973, pp. 58-67.

[3] Wyborny, W. and Requardt, G., "A New Aerodynamic Free Flight Testing System for Six-Component Measurements in Short Duration Wind Tunnels," AIAA Paper 74-613, Bethesda, Md., 1974.

[4] Wyborny, W. and Kabelitz, H.-P., "Funktionsuntersuchungen und erste Versuchsergebnisse im Stosswellenwindkanal mit freifliegendem Kolben," DLR FB 65-43, 1965.

[5] "Flugmechanik, Begriffe, Benennungen, Zeichen, Grundlagen," Normenstelle Luftfahrt LN 9300, 1970, Bl. 1.

Flux of Cosmic Ray Heavy Nuclei Enders behind Low Shielding

O. C. Allkofer*
CERN, Geneva, Switzerland
and
W. Heinrich*
Gesamthochschule Siegen, Germany

FOR manned space flights, especially in lengthy missions, the consideration of cosmic ray heavy nuclei is necessary. The phenomenon of the light flashes, which were for the first time seen by the Apollo astronauts, emphasized the particular importance of these particles which can deposit large amounts of energy near their path through matter.

Received June 7, 1974; revision received September 11, 1974. We wish to thank the coinvestigators of the Biostack-Experiment (Principal Investigator, H. Bücker) for supporting us with the fluxes of heavy nuclei measured inside the stack.

Index category: Space Medicine.

*Physicist.

Table 1 Constants for the determination of the number of stopping nuclei per cm^3 tissue hour and sterad by $N=N_0 \exp(-x/k)$ as a function of the absorbing material thickness x gcm^{-2}

Charge group	Depth of matter	Solar minimum		Solar maximum	
	[g cm^{-2}]	N_0[cm^3 tissue sr h]$^{-1}$	k[g cm^{-2}]	N_0[cm^2 tissue sr h]$^{-1}$	k[g cm^{-2}]
M	0 - 20	$9.50\,10^{-2}$	18.5	$2.85\,10^{-2}$	20.2
$6 \leq Z \leq 9$	20 - 40	$8.80\,10^{-2}$	20.0	$2.65\,10^{-2}$	21.4
H3	0 - 20	$4.10\,10^{-2}$	13.5	$1.05\,10^{-2}$	16.5
$9 \leq Z \leq 14$	20 - 40	$3.50\,10^{-2}$	15.3	$9.00\,10^{-3}$	18.7
H2	0 - 20	$6.95\,10^{-3}$	13.5	$1.95\,10^{-3}$	16.7
$15 \leq Z \leq 19$	20 - 40	$6.50\,10^{-3}$	14.0	$1.85\,10^{-3}$	17.5
H1	0 - 20	$1.85\,10^{-2}$	8.9	$5.50\,10^{-3}$	10.5
$20 \leq Z \leq 28$	20 - 40	$1.30\,10^{-2}$	10.7	$3.95\,10^{-3}$	12.6

The flux of heavy nuclei inside a space ship is dependent on the energy spectrum and the charge composition of the nuclei in free space and on the interaction properties of the nuclei with the material of the space ship. Two independent processes, energy loss and fragmentation, are responsible for the absorption of the nuclei. The energy loss by ionization is roughly proportional to (Z^2/E) (Z and E are charge and energy of the particle). We have measured the attenuation of the flux of heavy nuclei in the atmosphere and deduced from these results the fragmentation probabilities of heavy nuclei.[1]

Using these fragmentation probabilities and considering the energy loss by ionization, energy spectra of different charge groups of nuclei in absorber depths of 0-40 gcm^{-2} have been calculated from the primary spectra. For the period of minimum solar activity, the primary spectra measured by Webber and Ormes,[2] Freier and Waddington[3] and Bhatia et al.[4] were used, whereas for the period of maximum solar activity the spectra of the different charge groups were deduced from the He-spectrum of Mason[5] using the ratios of He to the heavy nuclei as given by von Rosenvinge et al.[6] respectively, following from the measurements of Webber et al.[7]

From the calculated spectra, the number N of stopping nuclei per cm^3 tissue sterad and hour as a function of the thickness x gcm^{-2} of the penetrated matter were deduced. The results can be expressed in the form:

$$N=N_o \exp\,(-x/k)$$

This description by an exponential law is only valid for restricted intervals of depth in matter. Table 1 shows the constants k and N_o for different intervals of depths x. These parameters are of value because with them one can calculate the number of stopping nuclei per cm^3 hour at any point $\vec{r}$ in a complicated volume.

If we assume omnidirectional incident nuclei, the expression is just:

$$N(\vec{r})=N_0 \int_0^{2\pi} \int_{-\pi/2}^{+\pi/2} \exp(-x(\vec{r},\theta,\zeta)/k)\sin\theta\, d\theta\, d\zeta$$

where $x(\vec{r},\theta,\varphi)$ is the absorber thickness shielding a volume at the point $\vec{r}$ against free space in direction θ and φ.

For comparision with the calculated fluxes measurements in the Biostack I experiment, flown on board Apollo 16 at nearly solar maximum activity were used.[8] This Biostack had a cylindrical shape with a depth and a diameter of about 9 cm. It consisted of different biological layers embedded between layers of nuclear emulsion and of plastic detectors. Figure 1 shows the measured fluxes[9] of nuclei with charges $Z \geq 6$ that produce visible tracks (REL$\geq 10^3$ Mev g^{-1} cm^2), respectively, stop in the foils and the fluxes of nuclei producing tracks with two etchable cones in a plastic foil.[10] The last scanning condition corresponds to an REL of about $1.5\,10^3$ Mev g^{-1} cm^2 for the M-group ($6 \geq Z \leq 9$). REL (restricted energy loss) gives the share of LET (linear energy transfer) that causes track formation in the plastic detectors. For a definition in detail, see Ref. 11.

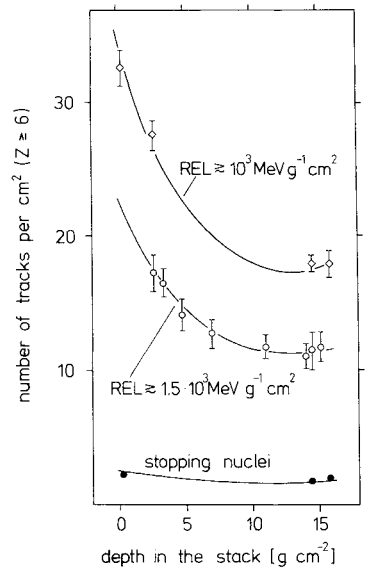

Fig. 1 The number of tracks of heavy nuclei measured in the Biostack for: ◇ all etchable tracks[9] (REL$\geq 10^3$ Mev g^1 cm^2); ○ etchable tracks with two etched cones per foil[10] (REL$\geq 1.5\,10^3$ Mev $g^{-1}cm^2$); • tracks of stopping nuclei.[9] The curves are calculated values.

Table 2 Absorbing material around the Biostack in the Apollo 16 space flight as used for the calculation of the particle flux in the stack

Direction of incidence of the heavy nuclei	Absorber thickness [g cm^{-2}]	
	Above the stack	Around the stack
Through the wall of the space ship	3	6
through the cabin and the instrumentation	15	15

For each charge group, the fluxes of the calculated energy spectra were summed up in the energy intervals equivalent to the scanning conditions. The track density was obtained by integration over all angles of incidence. The absorbint material of the space ship was roughly approximated by the assumption that the Biostack was surrounded cylindrically by matter. As the Biostack was orientated with the top side towards the wall of the space ship, the direction of incidence was separated for the two cases shown in Table 2.

Difficulties arise with the calculation of the absolute track density in the Biostack. The threshold of REL for particle registration by the plastic foils increases for nuclei that hit the foils under flat angles. Very flat tracks can not be seen at all because they are etched away with the surface of the foil. An investigation of the influence of the threshold of REL and of the interval of the angle of incidence on the calculated intensities showed that the shape of the absorption curves is scarcely altered by the variation of these two parameters.

But only the absolute frequency of thr tracks. Therefore the absorption curves of Fig. 1 were calculated assuming a threshold of REL = 10^3 Mev g^{-1} cm^2 and omitting tracks of particles incident under angles flatter than 15° to the plastic foils. The absolute intensities were normalized so that the differences to the measured values are a minimum.

References

[1] Allkofer, O. C. and Heinrich, W., "Attenuation of Cosmic Ray Heavy Nuclei Fluxes in the Upper Atmosphere by Fragmentation," Nuclear Physics, B 71, 1974, pp. 429-438.

[2] Webber, W. R., and Ormes, J. F., "Cerenkov-Scintillation Counter Measurements of Nuclei Heavier than Helium in the Primary Cosmic Radiation," *Journal of Geophysical Research,* Vol. 72, Dec. 1967, pp. 5957-5956.

[3] Freier, P. S. and Waddington, C. J., "The Energy Spectrum of the $Z \geq 20$ Component of the Cosmic Radiation," *Canadian Journal of Physics,* Vol 46, 1968, p. 578.

[4] Bhatia, V. S., Chahan, V. S., Pabbi, S. D., and Biwas, S., "Charge and Energy Spectra of Cosmic-Ray Nuclei with $Z = 10—28$," *Canadian Journal of Physics,* Vol 46, Oct. 1968, p. 588.

[5] Mason, G. M., "Interstellar Propagation of Galactic Cosmic-Ray Nuclei $2 \leq Z \leq 8$ in the Energy Range 10-1000 MeV per Nucleon," *The Astrophysical Journal,* Vol. 171, Jan. 1972, pp. 139-161.

[6] Von Rosenvinge, T. T., Webber, W. R., and Ormes, J. F., "A Comparison of the Energy Spectra of Cosmic Ray Helium and Heavy Nuclei," *Astrophysics and Space Science,* Vol. 5, 1969, pp. 342-359.

[7] Webber, W. R., Damle, S. V., and Kish, J., "Studies of the Chemical Composition of Cosmic Rays with $Z = 3$-30 at High and Low Energies," *Astrophysics and Space Science,* Vol. 15, 1972, p. 245.

[8] Bücker, H., et al., *The Biostack Experiment on Apollo 16," Cospar, Life Science and Space Research XI,* Akademie-Verlag, Berlin, 1973, pp. 295-305.

[9] Enge, W., et al., *Biostack Experiment M-211, Apollo 16,* Second Quarterly Rept., Dec. 1972.

[10] Bücker, H., "Biophysikalische Raumforschung," Frankfurt, private communication, Oct. 1973.

[11] Benton, E. V., U. S. Naval Radiological Defense Lab., San Francisco, Calif., Rept. USN RDL-TR-68-14, 1968.

A Miniature Solid State Pressure Transducer for R/V Flight Test Applications

J. M. Cassanto*

General Electric Company, Philadelphia, Pa.

Introduction

THE purpose of this Note is to present the results of a flight experiment which has demonstrated the feasibility of a miniaturized solid-state pressure sensor to measure steady-state pressures in an R/V flight test application. These recently developed solid-state transducers operate on the strain gage principle and are an order of magnitude smaller than potentiometer type transducers utilized in past and current R/V flight vehicles. Since R/V's invariably are weight and volume limited, use of the miniaturized sensor allows more flight pressure measurements to be made. In addition, pressure data can now be obtained in the nose region of R/V's (an area hitherto inaccessible for pressure measurements because of volume constraints or time lag effects) if long pressure tubing were utilized in conjunction with conventional "pot" sensors.

Received August 14, 1974; revision received October 2, 1974.

Index categories: LV/M Flight Testing; LV/M Aerodynamics.

*Project Engineer, Re-entry and Environment Systems Division. Member AIAA.

An extensive development program has been in existence at GE/RESD since late 1971 to gain experience with miniaturized solid-state pressure sensors for flight test applications, and has been structured to take maximum advantage of existing wind tunnel programs on which "piggyback" measurements of both steady-state and fluctuating pressures were made. In addition, other tests were conducted consisting of: static calibration, accuracy/resolution and linearity, time response, temperature effects, and long-term stability (results of the development program are presented in Refs. 1 and 2). The present flight results represent the culmination/end product of the development program.

Sensor Description

The miniaturized solid state pressure sensor under consideration is manufactured by the Kulite Corporation[3] and is compared to a typical conventional potentiometer type pressure sensor in Fig. 1. The solid state pressure sensor uses a (semiconductor) strain gage having a four-active element bridge circuit as an integral part of the diffused silicon diaphragm. The transducer has a reference pressure tube to permit operation as a differential or an absolute pressure sensor. The sensors utilized in the present program were all absolute units and employed a sealed reference pressure.

In addition to the obvious size advantage, the solid state sensor has a high enough frequency response to measure fluctuating as well as steady-state pressures. This represents an advantage over conventional "pot"-type sensors since the solid state sensor can be used to determine both frustum or nose tip loading and frustum or nose tip transition. Figure 2 shows the sensor packaged in the screw thread configuration with protector screen utilized for the flight experiment.

Flight Results

Although the prime forcing function for the new minaturized solid state sensor is pressure measurements on or near the nose tip of re-entry vehicles, the purpose of the present experiment was to demonstrate flight feasibility only and frustum pressure measurements were "piggybacked" on two R/V flights. Data will be presented herein on only one flight to illustrate the results. Complete flight results can be obtained in Ref. 1.

The re-entry vehicle for the second flight experiment was a slightly blunt slender cone and utilized an ablative heat shield

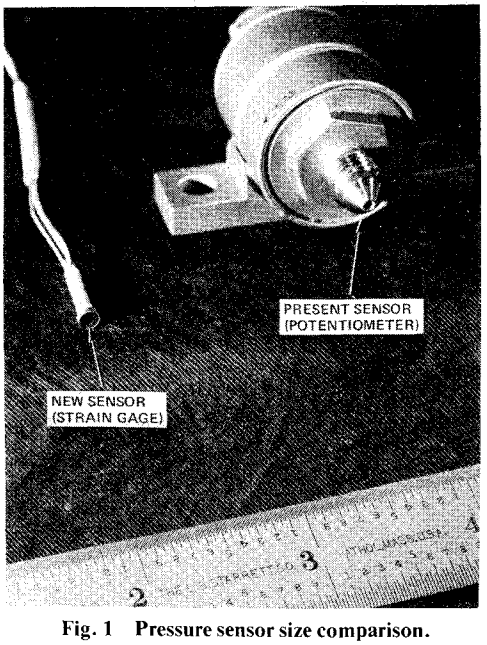

Fig. 1 Pressure sensor size comparison.